RSC Advances

ROYAL SOCIETY OF CHEMISTRY

www.rsc.org/advances

A novel and highly sensitive electrochemical monitoring for 4-nitrophenol on MnO_2 nanoparticles modified graphene surface

Shabi Abbas Zaidi*, Jae Ho Shin

Department of Chemistry, Kwangwoon University, Wolgye-Dong, Nowon-Gu, Seoul, 139-701, Korea

Correspondence:

E-mail: shabizaidi79@gmail.com

Tel : +82-2-940-8661

Fax: +82-29118584

Keywords: 4-Nitrophenol; reduced graphene oxide; Manganese dioxide (MnO_2) nanoparticles, electrochemical sensor

Abstract

4-Nitrophenol (4-NP) has been considered a deadly pollutant causing slow photosynthetic reactions, carcinogenicity and other related serious detrimental effects toward human and aquatic life. In this work, a novel, sensitive and reliable electrochemical sensor was prepared by electrodepositing manganese dioxide nanoparticles (MnO_2-NPs) over reduced graphene oxide (RGO) for the determination of 4-NP. The successful synthesis of graphene oxide (GO), reduced graphene oxide, and MnO_2-NPs were characterized by scanning electron microscopy (SEM). The electrochemical behavior of 4-NP at the MnO_2-RGO/GCE and various other modified electrodes were investigated and compared. It was observed that only MnO_2-RGO/GCE electrode exhibited well defined redox peak currents toward 4-NP. Under optimized conditions, the reduction peak current varies linearly with the concentration of 4-NP ranging between 0.02-0.5μM and 2-180 μM and a detection limit (LOD) of 10 nM (S/N=3) was estimated. Furthermore, the as-fabricated sensor displayed high selectivity, stability, reproducibility and excellent recoveries of 4-NP in various water samples spiked with 4-NP. Thus, the proposed method endorses an outstanding platform for the detection of 4-NP with great ease and reliability.

1. Introduction

The aromatic nitrocompounds are of primary importance and their use have been exploited tremendously due to their utilization in the synthesis of various types of pesticides, synthetic dyes, pharmaceuticals, paints and petrochemical products.[1,2] These compounds add undesirable color to water resources, preventing the penetration of sunlight, retarding photosynthetic reactions and affecting aquatic life and pose serious detrimental effects on living beings and plants. The discharge of these industrial waste effluents into the water bodies such as rivers, lakes, and ponds have inevitably resulted in an increased flux of toxic aromatic nitrocompounds.[3] Due to their toxic and prolonged effects, the U.S.A. environmental protection agency (EPA) has listed nitrocompounds as main pollutants and has enforced stringent regulations to control their discharge into water resources. In particular, the hazardous and highly toxic 4-nitrophenol (4-NP) is one of the most detrimental among pollutants various nitrocompounds. It has been reported as a potential carcinogen, mutagen and teratogen. Acute ingestion of 4-NP also causes severe headaches, drowsiness, nausea and cyanosis.[4,5] Hence, its utilization requires strict control and monitoring in order to avoid adverse effects on living beings. Therefore, a simple and robust analytical method is necessary for accurate and reliable measurements of 4-NP.

Reviewing the reports on 4-NP measurements, it is confirmed that several methods such as capillary zone electrophoresis[6], high performance liquid chromatography[7], gas chromatography, (GC)[8], fluorescence[9], and spectrophotometry[10] have been developed successfully. These methods are routinely used and offer precise and accurate determination of 4-NP, but suffer from long response time, high cost of analysis, due to expensive instruments and tedious sample cleanup and pretreatment approaches.

The electrochemical technique usually offers greater sensitivity, in addition to its other outstanding features such as low cost, easy operation, fast response time and great potential for miniaturization and construction for portable equipment applications.[11-13] Hence, these excellent characteristics keep electrochemical techniques at the forefront.

In order to benefit from these facts, numerous electrochemical methods including molecularly imprinted polymer–carbon paste electrode[14], a graphene oxide modified electrochemical sensor[15,16], hydroxyapatite nanopowder modified GCE[17], poly(propyleneimine)-gold nanocomposite[18], and graphene-Au composite[19] based electrochemical sensors have been introduced. All of these methods were satisfactorily applied for the determination of 4-NP. However, the requisition of better electrochemical sensor for 4-NP utilizing novel intriguing materials which possess magnificent electrocatalytic properties is always a challenge.

In recent decades, there is an immensely growing interest in graphene chemistry due to its enormous potential in material synthesis at nanoscale. The features that make Graphene an ideal material are high surface area, extremely low noise and distinguished electrical and thermal conductivity. Moreover, the specific surface area of a single graphene sheet is 2630 $m^2 g^{-1}$, which is quite higher than that of activated carbons and carbon nanotubes. Therefore, graphene has made its niche in catalysts, sensors, and energy storing and composite materials research areas.[20-22] On the other hand, among several nanostructured metal oxides, manganese oxide (MnO_2) has been in news due to its superb electro-catalytic properties and fast response time to substrate and has been utilized to construct chemical sensors and biosensors.[23, 24]

In the present work, we have successfully exploited the unique features of graphene and MnO2 nanoparticles (MnO_2-NPs). Thus, an electrochemical sensor was prepared by simply electrodepositing MnO_2 NPs over reduced graphene oxide (RGO) at glassy carbon electrode

(GCE) for the detection of 4-NP. The as-fabricated 4-NP sensor exhibited excellent sensitivity and selectivity.

2. Material and Methods

2.1 Reagents

4-nitrophenol (4-NP), 2,4-dinitrophenol (2,4-DNP), 4-aminophenol (4-AP), Nonylphenol (NP) Bisphenol A (BPA), phenol, graphite powder, tetrahydrofuran (THF), sulphuric acid (~98% pure), dimethylformamide (DMF), Sodium nitrite ($NaNO_3$), Hydrogen peroxide (H_2O_2) and Potassium permanganate ($KMNO_4$) were obtained from sigma Aldrich. All other analytical grade chemicals were also purchased from Sigma Aldrich and used as received without further purification. Double-distilled water was used throughout the work.

0.1M PBS buffer (supporting electrolytes) was prepared by dissolving the appropriate amounts of sodium phosphate monobasic monohydrate ($NaH_2PO_4 \cdot H_2O$) and sodium phosphate dibasic dihydrate ($Na_2HPO_4 \cdot 2H_2O$) and NaCl. The sample solutions were freshly prepared before use by diluting the stock solution with appropriate amount of PBS buffer.

2.2 Apparatus

The morphologies of synthesized GO, RGO, and MnO_2-NPs were examined by field emission scanning electron microscopy (FESEM; JEOL-JSM-7600F). The electrochemical measurements were carried out using a CH Instruments (electrochemical analyzer 600B). The Fourier transform infrared (FTIR) spectroscopy was carried out at room-temperature in the range from 500-4000cm^{-1} with KBr pellet samples. For measurements, a simple three-electrode system was used where MnO_2-RGO/ GCE, Pt wire and Ag/AgCl were applied as working, counter and reference

electrodes, respectively. For all the experiments, 0.1 M phosphate buffer solution (PBS, pH 7.5) and a scan rate of 100mV/s were used unless specified.

2.3 Synthesis of Reduced graphene oxide

Firstly, the synthesis of graphene oxide (GO) was carried out by modifying the described method elsewhere.[25] Briefly, 1 g of graphite was added into 23 mL of 98% H_2SO_4, and stirred at room temperature for 24 h. Later, 100 mg of $NaNO_3$ was introduced into the mixture and stirred for 30 min and kept below 5°C in an ice bath. Then, 3 g of $KMnO_4$ was added slowly into the mixture. The resultant solution was heated to 35-40°C, and stirred for 30 min followed by addition of 46 mL of water and the reaction was continued for 30 min. Finally, 140 mL of water and 10 mL of 30% H_2O_2 were added into the mixture to stop the reaction. The unexploited graphite was removed by centrifugation and as-synthesized graphene oxide was dispersed into individual sheets in distilled water with a concentration of 1 mg/mL. The greyish black precipitates were washed with ethanol and water several times, and dried as graphene oxide sheets.

In order to synthesize reduced graphene oxide (RGO), an appropriate amount of GO was dissolved in distilled water and ultrasonicated for 20 minutes followed by mixing hydrazine and ammonia water (30%). The resulting solution was refluxed for 4 h at 90°C, centrifuged, and washed with distilled water thoroughly. After drying, a black color powder of RGO was obtained.

2.4 Sensor fabrication

Prior to 4-NP sensor fabrication, the glassy carbon electrode (GCE) surface was polished mildly with progressive alumina - water slurry on a polishing cloth, followed by thorough rinsing with distilled water. The GCE surface was electrochemically activated in a 0.01 M H_2SO_4 solution at

a scan rate of 100 mV/s using 12 times cyclic potential sweeps in the range of -1.0 to 1.0 V. A 1-2 μL of freshly prepared (1 mg/1 mL) dispersion of RGO in DMF was drop-casted into 4 successive aliquots onto the sensing area of GCE carefully using a pneumatic dispenser (EFD model 1000XL) and evaporated at 35±2◦C for 1-2 h to get a uniform and dry layer over active electrode surface for the 4-NP sensor surface modification (RGO/GCE).

For the synthesis of MnO_2-NPs over RGO modified GCE, the electrodeposition of MnO_2-NPs was carried out as reported elsewhere without any change.[24] Thus, the RGO/GCE was immersed in freshly prepared aqueous solution containing 10 mM $KMnO_4$ and 50 mM H_2SO_4 at 0.2 V for 300 s. After the electrodeposition procedure, the electrode was washed with water and dried at room temperature to achieve final 4-NP sensor (MnO_2-RGO/GCE). For comparison studies, RGO modified GCE (RGO/GCE), MnO_2-NPs modified GCE (MnO_2/GCE) were also prepared by simple drop casting and electrodeposition methods, respectively.

3. Results and discussion

3.1 Characterization of GO and RGO

The successful fabrication of GO, RGO and MnO_2-NPs were very crucial. Therefore, the morphology and chemical composition of GO and RGO were examined by SEM and FTIR spectroscopy respectively. The morphology of synthesized MnO_2-NPs was also confirmed by SEM analysis and electrochemical behavior effect of MnO_2-NPs was studied by cyclic voltammetry (CV).

Figure 1 shows the results obtained from SEM and FTIR analysis. As shown in Figure 1A, the exfoliated GO sheets have loosened due to the opening of carbon network at wedged and edge

surfaces by oxidation. On the other hand, Figure 1B displayed the SEM of RGO which indicated that RGO possessed intrinsic morphology with more wrinkled and gauze-like sheets surface providing extremely favorable and suitable surface for MnO_2-NPs electrodeposition. The figure 1C showed the synthesis of MnO_2-NPs successfully. It can be observed from SEM that the size of and MnO_2-NPs ranges between ~200nm to 400nm. This result is in close agreement as reported elsewhere.[24] The formation of GO and RGO nanomaterials were also confirmed by FTIR analysis and results have been assembled in Figure 1D (a & b). It showed that several well-defined peaks at 1063, 1398, 1620, 1720 and 3368cm^{-1} corresponding to different oxygen functionalities have been observed in the obtained FTIR spectrum of GO in figure 1D (a). The strong peak appeared at about 3368cm^{-1} is related to –OH which originates from stretching vibration. The appearance of another absorption peak at ~ 1720 confirm the presence of –COOH (stretching vibrations from C=O). The two peaks appeared at 1398 and 1063 cm^{-1} could be ascribed to the C-OH stretching vibrations and C-O-C stretching vibrations, respectively. In addition, a peak corresponding to unoxidized graphitic domains or the remaining sp2 character of graphite was also observed at 1600 cm^{-1}. It is clearly visible in Figure 1D (b) of RGO that no characteristic FTIR peaks were observed indicating ample reduction of oxygen functionalities which supported the successful synthesis of RGO. The FTIR spectrum of our graphene matches well with other previous reports in the literature.[26]

3.2 Electrochemical characterization of 4-NP sensor

In order to investigate the electrochemical behavior of as-fabricated sensor, the sensor electrode was characterized using $[Fe(CN)6]^{3-/4-}$ as redox probes by cyclic voltammetry (CV) shown in Figure 2. Figure 2 demonstrates that CVs of bare GCE (a), MnO_2/GCE (b), RGO/GCE (c) and MnO_2-RGO/GCE (d) electrodes were monitored in freshly prepared 1M $[Fe(CN)6]^{3-/4-}$ (1:1)

solution containing 0.1 M KCl at a scan rate of 100 mV/s. It can be observed that a well-defined redox couple peaks appeared at bare electrode (curve a). After the electrode modification with MnO_2-NPs, there was certainly an improvement in redox peaks current (curve b). When the electrode was coated with RGO, the redox peak currents were improved significantly owing to superior electro conduction ability of RGO (curve c). After the electrode modification with MnO_2-NPs, there was an improvement in redox current, but it was lower than RGO/GCE electrode. At MnO_2-RGO/GCE, the redox peak currents increased greatly, indicating the synergic effect from MnO_2 NPs and RGO (curve d). In addition, the peaks separation was reduced to some extent compared to curve (b) and (c). This can be attributed to better electrochemical reversibility, electrocatalytic activity, high conductivity, large specific surface area and synergistic effect of MnO_2-NPs and RGO compared to bare GCE, RGO/GCE, and MnO_2/GCE.

The figure 2B shows the electrocatalytic behavior of 4-NP at bare GCE and various modified electrodes analyzed by CV in only 0.1 M PBS (pH 7.5) containing 140 μM 4-NP. There was poor and irreversible response generated at bare GCE in the presence of 4-NP which exhibited almost negligible cathodic peak at ~ -0.22 V and poor anodic peak at about 0.2V (curve a), which suggested that direct electron transfer of 4-NP on bare GCE was very slow. At MnO_2/GCE (curve b), relatively increased cathodic peak shifted to higher potential at ~ -0.1 V and a broad anodic peak at about 0.3V (curve b) were observed due to increase electrocatalytic capability of MnO_2-NPs toward 4-NP. The curve (c) of figure 2B depicts the response of RGO/GCE toward 4-NP. It is visible that an improved cathodic peak at ~ -0.23V and somewhat broad anodic peak at about 0.2V were achieved. At MnO_2-RGO/GCE (curve d), a greatly enhanced redox current peaks at -0.28 and 1.5 V was achieved due to the reversible two-electron

oxidation reduction of the hydroxylamine group (-NHOH) to a nitroso group (-NO). Moreover, a large irreversible cathodic peak at ~ 0.05 was also generated from a four-electron irreversible reduction of the nitro group (-NO) to a hydroxylamine group (-NHOH) as clearly visible in curve (d). This suggested that incorporation of MnO_2-NPs with RGO had significant impact in the electrocatalytic behavior of 4-NP. There was a significant enhancement in reduction peak current as compared to oxidation peak current. In addition, the cathodic peak and anodic peaks potential shifted negatively to lower potential at -0.28V and 1.5V, respectively. Thus, the remarkable peak current enhancement and the negative shift of cathodic peak potential may be attributed to the high electron transfer rate, exemplary electrocatalytic, high conductivity performance and synergistic effect of MnO_2-NPs and RGO toward 4-NP. These results were in close agreement with other reports on 4-NP.[15, 16]

3.3 Optimization of experimental conditions

In order to realize the maximum efficiency from as-fabricated 4-NP sensor, the RGO loading content and buffer pH were optimized as shown in figure 3. Figure 3A shows that 1 mg/mL of RGO loading provided highest response. Thus, it was used in this study. In addition, it was observed in our study that small multiple aliquots (~1-2μL) with lower concentrations (1 mg/ mL) offered superior current signals as compared to single coating with highly concentrated dispersion of RGO in DMF. Gradually increasing the aliquots from 1 to 4, the effective surface area for 4-NP reduction was increased, but further increase in aliquots decreased in reduction current of 4-NP, indicating that film thickness was high affecting current efficiency. Hence, 4 successive drop-coating of RGO (1mg/mL) were found to be suitable.

For the pH optimization experiments shown in figure 3B, various buffer pH (pH 4, 5, 6, 7, 7.5, 8, and 9) were analyzed. Increasing the buffer pH from 4 to 7.5, the 4-NP redox current increases to maximum, but it began decreasing after pH 7.5 to 9. The buffer pH 7.5 exhibited better results considering redox current responses and redox potential. Thus, buffer pH 7.5 was used throughout the study.

3.4 Analytical performance of 4-NP Sensor

Under optimized conditions such as RGO loading and buffer pH (pH 7.5), the linear sweep voltammetry (LSV) responses of reduction peak at -0.28V of 4-NP were obtained at various concentrations from 0.02 µM to 180 µM and have been reported in Figure 4. The Figure 4A clearly showed that the current responses were increased consistently with the increase in 4-NP concentration. Figure 4B presents calibration plot obtained for 4-NP between 0.02 µM to 180 µM. The plot of peak current vs. 4-NP concentration consisted of two linear segments in the concentration ranges of 0.02-0.5µM ($y=-8.753\times10^{-5}-3.566\times10^{-5}.C$) and 2-180 µM ($y=-1.286\times10^{-4}-3.745\times10^{-6}.C$, where C is the concentration) with correlation coefficients values of 0.991 and 0.995, respectively. The detection limit (LOD) for 4-NP was determined to be 10 ± 2 nM (S/N=3, RSD < 5%) based on three measurements. It was found that our results were comparable or even better in terms of sensitivity and linear range with other reported methods.[15, 27, 28]

3.5 Interference study, stability, reproducibility analysis, and analytical application

The as-proposed 4-NP sensor was evaluated for its selectivity in the presence of some structurally related compounds including 2,4-dinitrophenol (2,4-DNP), 4-aminophenol (4-AP), nonylphenol (NP), Bisphenol A (BPA), phenol, as possible interfering compounds under optimized experimental conditions. As shown in Figure 5, the signals of all the compounds were

remarkably lower than the 4-NP, even though the concentration of 4-NP was half (50μM) of other interfering compounds (100μM). Thus, the poor response of interfering compounds supports that the fabricated 4-NP sensor electrode is quite selective and suitable for the determination of 4-NP. Moreover, the reduction peaks of interfering compounds were detected toward more positive (~10-15mV) potential as compared to 4-NP peak.

Furthermore, the stability of proposed as-fabricated sensor was investigated by comparing daily responses obtained after storing it in working electrolyte (0.1M PBS, pH-7.5 at ambient temperature). It was observed that the sensor retained almost 98% of its sensitivity for over 5 weeks. However, the response was decreased to approximately 87% and 76% in 6^{th} and 7^{th} week, respectively. After 7^{th} week, the sensor lost almost half of its sensitivity which could be attributed to the leaching of modification material over electrode surface.

To characterize the repeatability of 4-NP sensor results, 10 repetitive measurements were carried out. The results showed a RSD of 0.5 % for 4-NP determination, indicating that the modified sensor was not subjected to any kind of surface fouling during analysis.

The validity and analytical applicability of proposed method were assessed in various water samples collected from different sources by spiking with different concentrations of 4-NP. Prior to spiking, the water samples were investigated to confirm the presence of 4-NP but no samples showed positive result. It is clear from Table 1 that excellent recoveries upto 97.4% of the added 4-NP standards were achieved under permissible RSD limits without any matrix interferences. In addition, it was found that the results obtained from as-proposed method were in close agreement with the value achieved by HPLC method.[29] The demonstrated results substantiated that proposed method is a simple, robust, reliable procedure for 4-NP determination in real samples too.

Table 2 displays the results compilation obtained for the determination of 4-NP from this method and other reported works. It can be deduced from table 2 that proposed electrode sensor performance is comparable or better than other sensors in terms of detection limit linear range indicating that this could be an excellent monitoring method for accurate and reliable analysis for 4-NP.

4. Conclusion

A novel, sensitive and robust approach for the fabrication of 4-NP electrochemical sensors using MnO_2-NPs and RGO modified glassy carbon electrode was proposed. The fabricated sensor exhibited remarkable improvement in the kinetics of the electron transfer for 4-NP, excellent electrocatalytic activity towards the 4-NP, long-term stability and quantitatively reproducible analytical performance in various spiked water samples. The results clearly indicate that this approach is a potential and promising strategy for reliable and sensitive determination of 4-NP in polluted samples.

Acknowledgement

This work is supported by the research fund from Kwangwoon University in 2015.

References

1. G. Busca, S. Berardinelli, C. Ressini, and L. Arrighi, *J. Hazard. Mater.,* 2008, **160**, 265.
2. Z. Liu , J. Du, C. Qiu, L. Huang, H. Ma, D. Shen, and Y. Ding, *Electrochem. Commun*., 2009, **11**, 1365.
3. P. Mulchandani, C.M. Hangarter, Y. Lei, W. Chen, and A. Mulchandani, *Biosens. Bioelectron.*, 2005, **21**, 523.
4. E. Lypczynska-Kochany, *Chemosphere*, 1991, **22**, 529.
5. US Environmental Protection Agency, 4-Nitrophenol, Health and Environmental Effects Profile No. 135, Washington, DC, 1980
6. X. Guo, Z. Wang, and S. Zhou, Talanta, 2004, **64**, 135.
7. R. Belloli, B. Barletta, E. Bolzacchini , S. Meinardi, M. Orlandi, and B. Rindone, *J. Chromatogr. A*, 1999, **846**, 277.
8. K. Nick, and H. F. Scholer, *Fresenius J. Anal. Chem.,* 1992, **343,** 304.
9. W. Zhang, and C.R. Wilson, *Talanta,* 2008, **74**, 1400.
10. X. Lin, Y. Chen, S. Li, Anal. Methods, 5 (2013) 6480.
11. R. Nissim, and R.G. Compton, *ChemElectroChem*, 2014, **1**, 763.
12. A.O. Simm, C.E. Banks, and R.G. Compton, *Electroanalysis*, 2005, **17**, 1727.
13. S.A. Zaidi, *Int. J. Electrochem. Sci.,* 2013, **8,** 9936.
14. T. Alizadeh, M.R. Ganjali, P. Norouzi, M. Zare, and A. Zeraatkar, Talanta, 2009, **79,** 1197.
15. J. Li, D. Kuang, Y. Feng, F. Zhang, Z. Xu , and M. Liu, *J. Hazard. Mater.*, 2012, **201–202**, 250-259.
16. A. Arvinte, M. Mahosenaho, M. Pinteala, A.M. Sesay, and V. Virtanen, *Microchim. Acta*, 2011, **174**, 337.
17. H.Yin, Y. Zhou, S. Ai, X. Liu, L. Zhu, and L. Lu, *Microchim. Acta*, 2010, **169,** 87.
18. T. Ndlovu, O.A. Arotiba, R.W. Krause, and B.B. Mamba, *Int. J. Electrochem. Sci.,*2010, **5,** 1179.
19. W. Zhang, J. Chang, J. Chen, F. Xu, F. Wang, K. Jiang, and Z. Gao, *Res. Chem. Intermed.,* 2012, **38,** 2443.
20. M. Pumera, A. Ambrosi, A. Bonanni, E.L. Khim Chng, and H. L. Poh, *Trends Anal. Chem.,* 2010, **29**, 954.
21. S.A. Zaidi, *Int. J. Electrochem. Sci., 2013,* **8**, 11337.

22. S.A. Zaidi, and J.H. Shin, *Int. J. Electrochem. Sci., 2014,* **9**, 4598.
23. Y.H. Bai, J.J. Xu, and H.Y. Chen, *Biosens. Bioelectron.,*2009, **24,** 2985.
24. G. Yu, Q. Zhao, W. Wu, X. Wei, Q. Lu, Talanta (2015) http://dx.doi.org/10.1016/j.talanta.2015.06.037
25. S. Stankovich, D.A. Dikin, R.D. Piner, K. A. Kohlhaas, A. Kleinhammes, Y. Jia, Y.Wu, S. T. Nguyen, and R. S. Ruoff, Carbon, 2007, **45**, 1558.
26. B. Unnikrishnan, S. Palanisamy, and S.M. Chen, *Biosens. Bioelectron., 2013,* **39**, 70.
27. C. Yang, *Microchim. Acta., 2004,* **148**, 87.
28. R.C.S. Luz, F.S. Damos, A.B. Oliveira, J. Beck, and L.T. Kubota, *Talanta*, 2004, **64,** 935.
29. J.H. Li, G.R. Li, H.B. Tang, X.Y. Xu, Y.F. Ouyang, Y.S. Wang, and H.M. Yang, *Chin. J. Spectrosc. Lab.*, 2011, **28**, 782-786.
30. R. Madhu, C. Karuppiah, S.M. Chen, P. Veerakumar, and S.B. Liu, *Anal. Methods,* 2014, **6**, 5274-5280.
31. Y. Tang, R. Huang, C. Liu, S. Yang, Z. Lu and S. Luo, *Anal. Methods,* 2013, **5**, 5508-5514.
32. J. Liu, Y. Chen, Y. Guo, F. Yang, and F. Cheng, *J. Nanomater.,* 2013, **2013,** Article ID 632809, 6 pages, http://dx.doi.org/10.1155/2013/632809
33. Y. Gu, Y. Zhang, F. Zhang, J. Wei, C. Wang, Y. Du, and W. Ye, *Electrochim. Acta,* 2010, **56,** 953-958.
34. W. Huang, C. Yang, and S. Zhang, *Anal. Bioanal. Chem.*, 2003, **375**, 703-707.
35. A. Niaz, J. Fischer, J. Barek, B. Yosypchuk, Sirajuddin, and M.I. Bhanger, *Electroanalysis, 2009,* **21,** 1786-1791.
36. S. Huang, Y. Zhou, Y. Gao, L. Xu, and H. Jiang, *Sens. Transducers*, 2015, **188**, 33-39.

Table 1 Determination of spiked 4-NP in various water samples by MnO_2-RGO/GCE.

Samples	Added[a] (μM)	Found		Recovery[b] (%)	RSD (%)[b]
		Proposed method	HPLC method[c]		
Drinking water	2	1.90	-	95.00	2.37
	25	24.20	24.50	96.80	1.45
	100	95.70	94.00	95.70	2.07
Underground water	2	1.90	-	93.50	1.34
	20	19.5	20.26	97.50	1.03
	100	94.90	-	94.90	1.93
Domestic sewage	2	1.91	2.10	95.50	1.4
	25	24.36	25.28	97.40	1.32
	100	95.00	94.35	95.00	1.90
Pond water	2	1.93	-	96.50	1.08
	10	9.57	9.77	96.00	1.21
	130	124.63	125.40	98.20	1.28

[a] Average value of three measurements

[b] Average Value for proposed method

c Only available values provided

Table 2 Comparison of the performances of different electrochemical sensors for 4-NP with proposed method.

Electrode modifications	Linear Ranges (μM)	Detection limit (μM)	References
biomass-derived AC[a]	1- 500	0.16	30
RGO/Au NP composite	0.05 - 2	0.01	31
β-CD-GNs/GCE[b]	5 - 400	0.3	32
Nano-Cu_2O/Pt electrode	10 -1000	0.1	33
MWNT-Nafion/GCE	0.1 - 10	0.04	34
GO/GCE	0.1- 120	0.02	15
AgA-PE[c]	0.2 -100	0.3	35
PSS-RGO/PAMAM-AuNPs[d]	5.0 - 515	1.8	36
MnO_2-RGO/GCE	0.02-0.5 & 2-180	0.01	this work

[a] biomass-derived activated carbon

[b] β-cyclodextrin functionalized graphene nanosheets

[c] Silver amalgam paste electrode

[d] poly sodium 4-styrenesulfonate functionalized reduced graphene oxide and polyamidoamine dendrimer protected gold nanoparticles

Figure Captions

Figure 1. SEM images of (A) GO, (B) RGO, (C) MnO_2 Nanoparticles. (D) FTIR spectra of GO (a), and RGO (b).

Figure 2. CVs (A) of bare GCE (a), RGO/GCE (b), MnO_2/GCE (c), and MnO_2-RGO/GCE (d) in 1M $[Fe(CN)6]^{3-/4-}$ (1:1) solution containing 0.1 M KCl. CVs (B) of bare GCE (a), MnO_2/GCE (b), RGO/GCE (c), and MnO_2-RGO/GCE (d) in 140µM 4-NP solution. The scan rate of CV is 100 mV/s.

Figure 3. The effect of RGO loading (A) and pH of buffer (B) on MnO_2-RGO/GCE sensor. Experimental conditions: 0.1M PBS (pH 7.5), concentration of 4-NP; 140µM, and scan rate; 100mV/s.

Figure 4. LSV responses of 4-NP to different concentration with MnO_2-RGO/GCE sensor at (a) Blank (b) 0.02 µM, (c) 0.1µM, (d) 0.25µM, (e) 0.4µM, (f) 0.5µM, (g) 2µM, (h) 10µM, (i) 25µM, (j) 50µM, (k) 70 µM, (l) 95 µM (m) 140, and (n) 180 µM. Experimental conditions: 0.1M PBS (pH 7.5), scan rate; 100mV/s (Inset shows the linear fit between 0.02 to 0.5 µM concentration of 4-NP).

Figure 5. Current responses of 4-NP and interferents on MnO_2-RGO/GCE sensor. Experimental conditions: 0.1M PBS (pH 7.5), scan rate; 100mV/s, Concentration; 4-NP (50µM), and all other interferents were 100 µM.

Figures

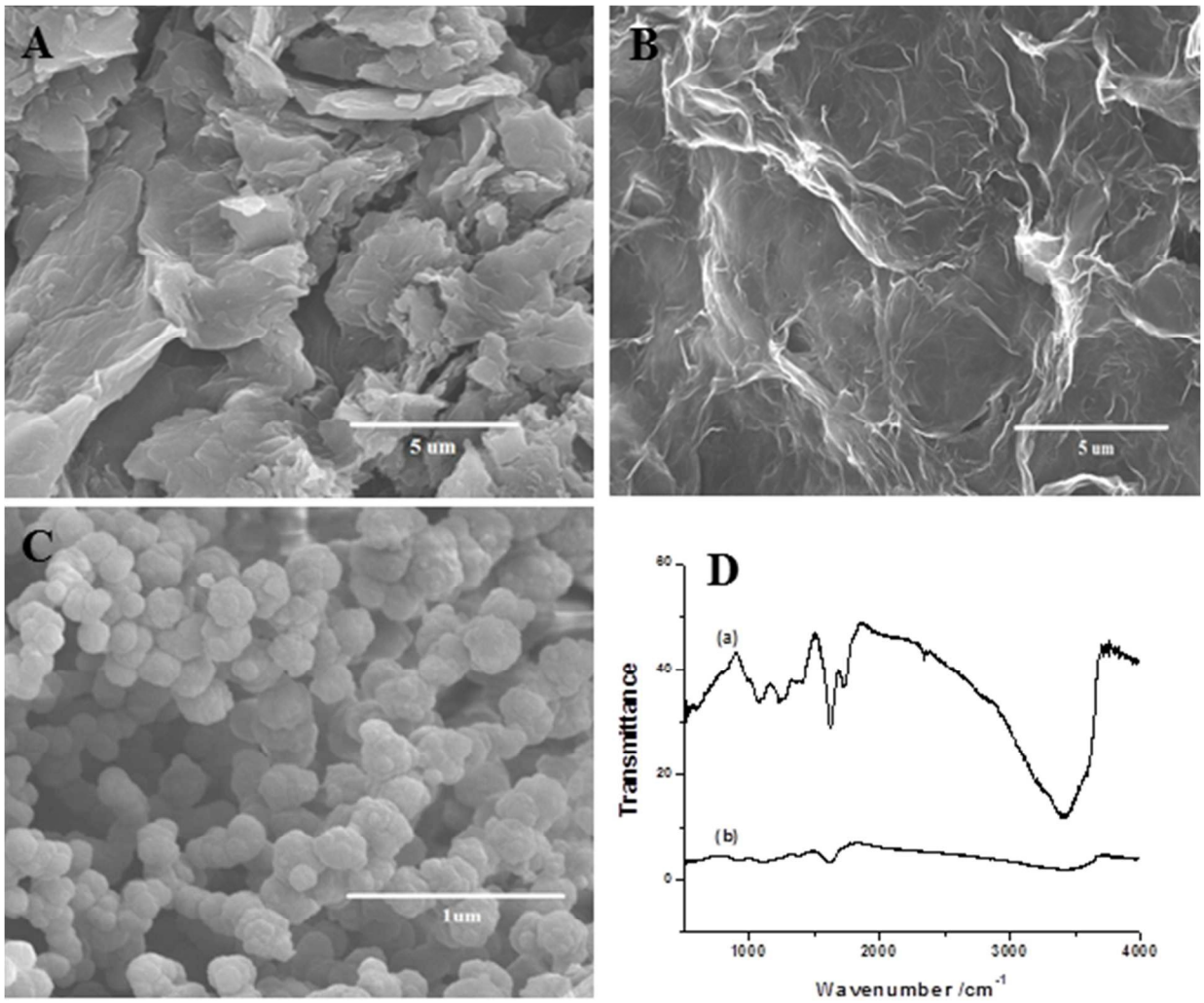

Figure 1

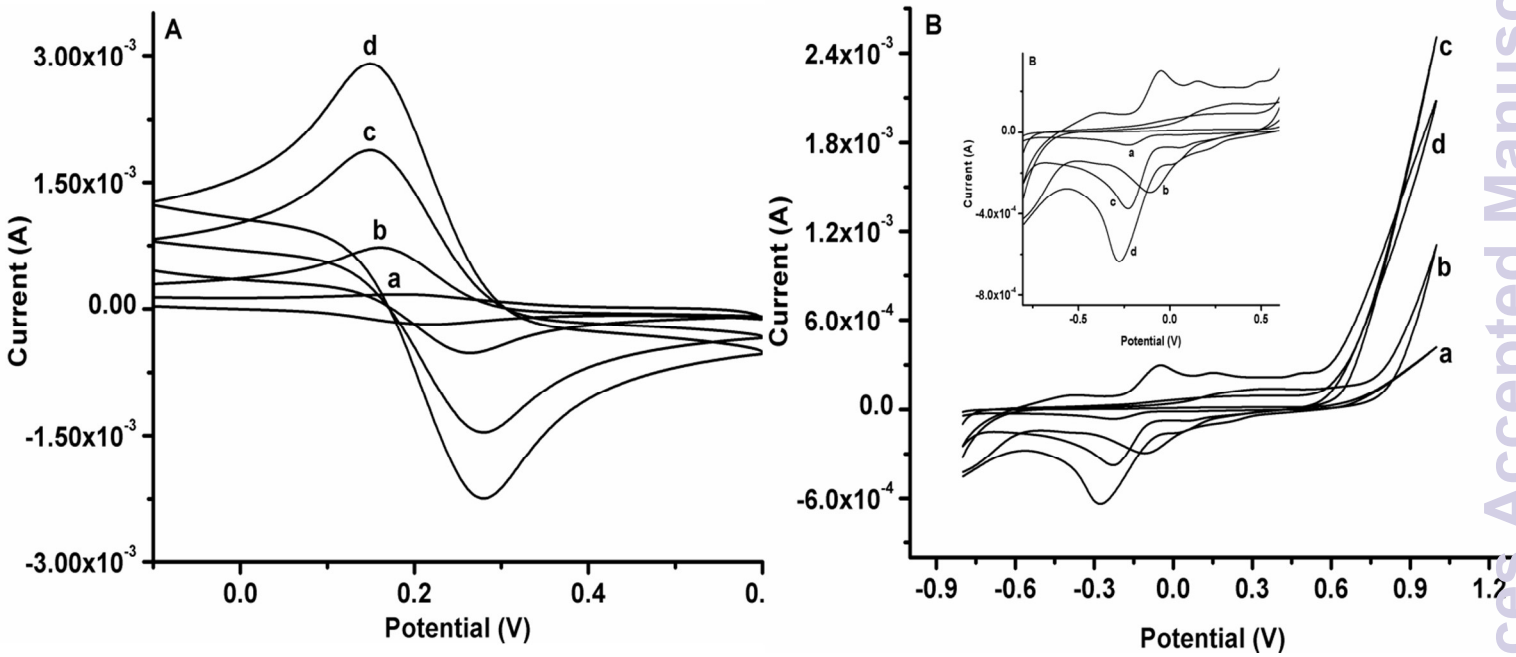

Figure 2

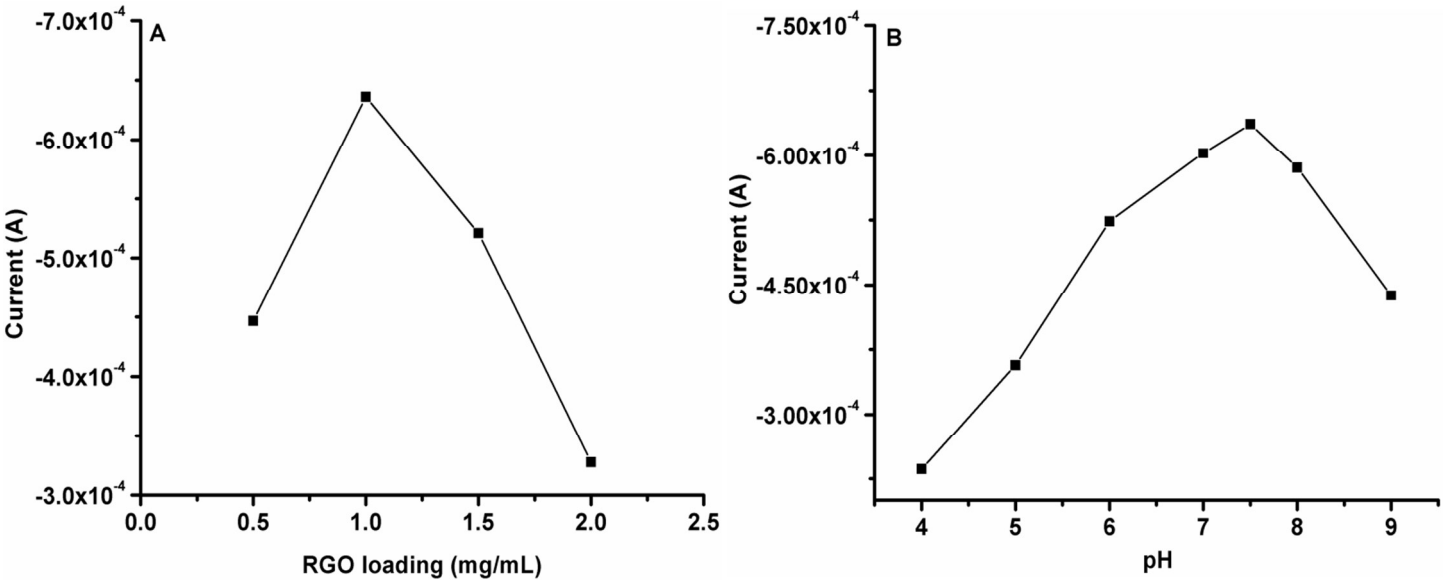

Figure 3

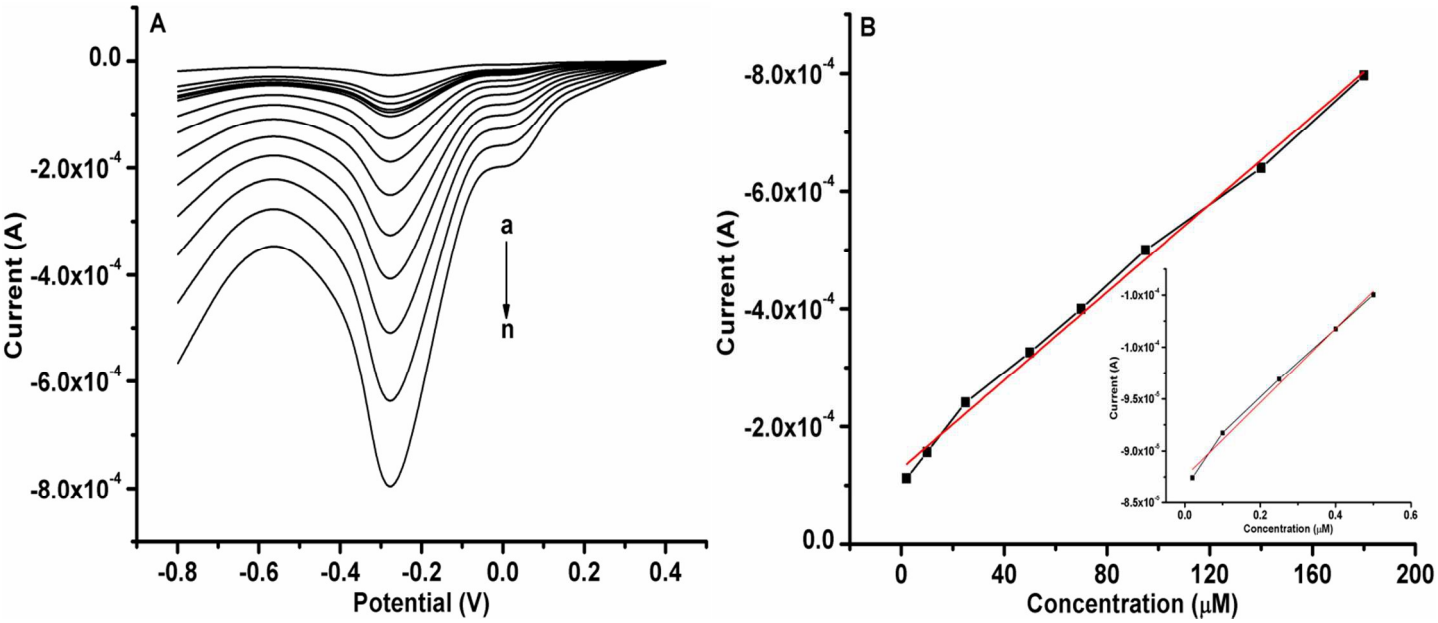

Figure 4

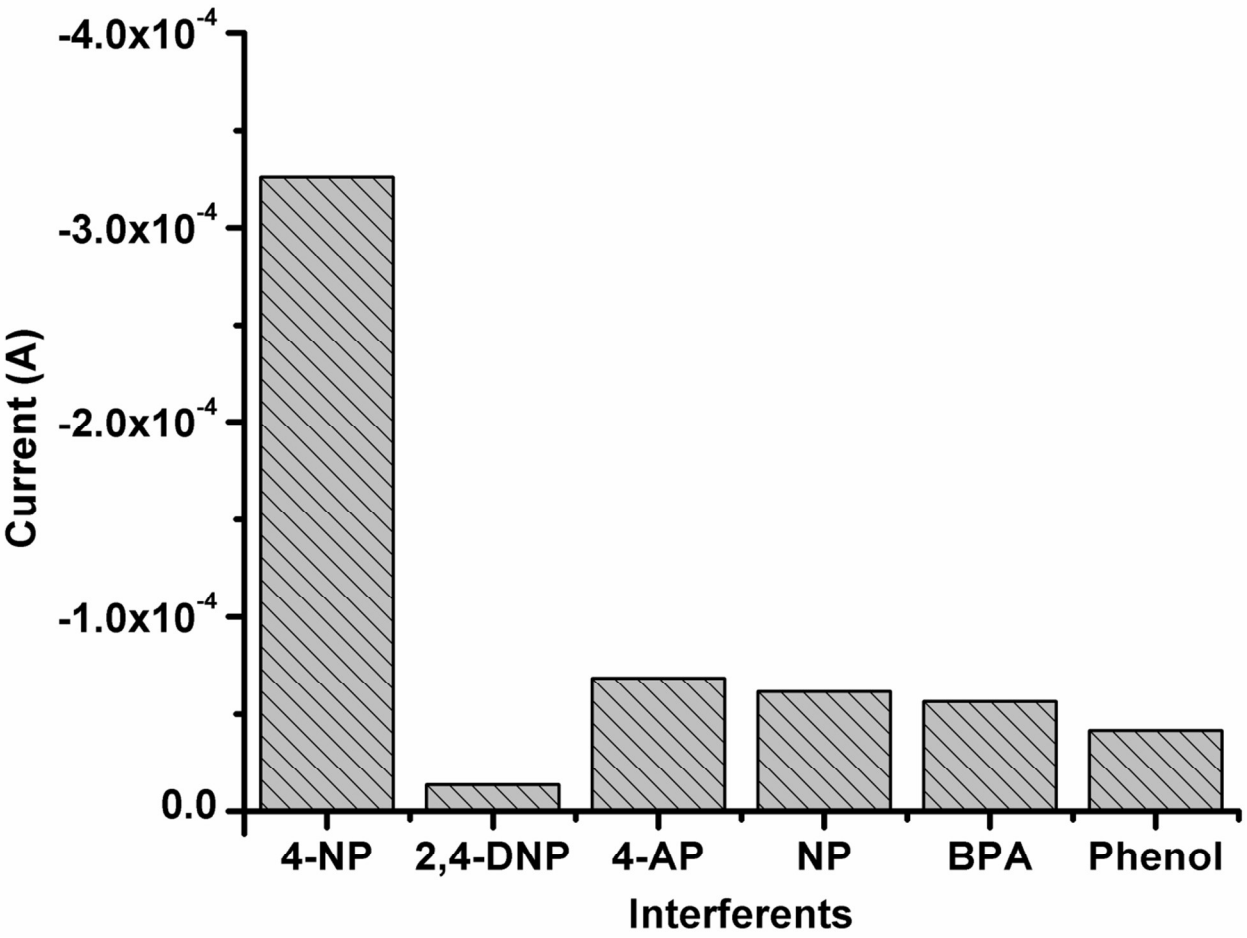

Figure 5